THE AMERICAN SOCIETY OF MECHANICAL ENGINEERS
345 E. 47th St., New York, N.Y. 10017

94-GT-67

FILM COOLING OF THE GAS TURBINE ENDWALL BY DISCRETE-HOLE INJECTION

M. Y. Jabbari, K. C. Marston,[1] E. R. G. Eckert, and R. J. Goldstein
Department of Mechanical Engineering
University of Minnesota
Minneapolis, Minnesota

ABSTRACT

Film cooling performance for injection through discrete holes in the endwall of a turbine blade is investigated. The effectiveness is measured at sixty locations in the region covered by injection. Three nominal blowing rates, two density ratios, and two approaching flow Reynolds numbers are examined. Analysis of the data reveals that even sixty locations are insufficient for the determination of the field of film cooling effectiveness with its strong local variations. Visualization of the traces of the coolant jets on the endwall surface, using ammonium-diazo-paper, provides useful qualitative information for the interpretation of the measurements, revealing the paths and interaction of the jets which change with blowing rate and density ratio.

NOMENCLATURE

A	total cross sectional area of injection holes (14 A_j)
A_j	cross sectional area of injection hole ($\pi D^2/4$)
c	chord length (16.91 cm, Fig. 1a)
C_i	approaching flow concentration
C_{iw}	impermeable wall concentration
C_j	injected flow concentration (the same for all jets)
D	injection hole diameter (1.905 mm, the same for all holes)
h	heat transfer coefficient
I_j	momentum ratio
L	length of the injection hole (L/D=15.77)
$\dot{m}$	total mass flow rate of coolant ($\sum_{j=1}^{j=14} \dot{m}_j$)
$\dot{m}_j$	mass flow rate of a single coolant jet (varies with holes)
M_j	blowing rate of a single jet ($\dot{m}_j$ / A_j) / ($\rho_\infty u_\infty$)
$\tilde{M}$	nominal blowing rate ($\dot{m}$ / A) / ($\rho_i u_i$), see Table 1
$P_{i,s}$	approaching flow static pressure
$P_{i,t}$	approaching flow total pressure
P_w	wall pressure
q_w	wall heat flux
R	density ratio (ρ_j/ρ_i)
Re_c	Reynolds number ($u_i c/\nu_i$)
T_{aw}	adiabatic wall temperature
T_j	injectant temperature
T_r	recovery temperature
T_w	wall temperature
u_i	approaching flow velocity (≈ 8.2 or 11.8 m/s)
u_∞	freestream velocity (varies with hole location)
η	film cooling effectiveness
η_{iw}	impermeable wall effectiveness
ν_i	kinematic viscosity of approaching flow
ρ_i	approaching flow density
ρ_j	injectant density (in plenum chamber)
ρ_∞	freestream density (≈ ρ_i)
χ	distance from downstream edge of injection hole along a row (Fig. 1b)

INTRODUCTION

Designers of aircraft engines strive to increase engine operating temperatures in order to attain higher thrust and improved efficiency. The main limitation on higher temperatures is the structural integrity of engine parts, especially those subject to high stresses. Uncooled metal alloys are not strong enough to withstand the severe conditions within the engine; therefore components must be cooled to avoid structural failure. One popular method used to maintain surface temperatures at acceptable levels is film cooling.

In film cooling, a secondary or coolant flow is injected into the boundary layer through a slot or an array of holes in the surface to be protected. The coolant serves to decrease the temperature in the boundary layer for some distance downstream of injection. The temperature which an adiabatic wall would assume in this process is called the adiabatic wall temperature, T_{aw}. It is conventionally described by a dimensionless parameter; the film cooling effectiveness:

$$\eta = (T_{aw} - T_r) / (T_j - T_r) \quad (1)$$

T_j in this equation denotes the temperature with which the coolant

[1] Presently at IBM Corporation, 522 South Road, Poughkeepsie, NY 12601

Presented at the International Gas Turbine and Aeroengine Congress and Exposition
The Hague, Netherlands — June 13–16, 1994
This paper has been accepted for publication in the Transactions of the ASME
Discussion of it will be accepted at ASME Headquarters until September 30, 1994

jet is injected into the boundary layer and T_r is the recovery temperature which the wall assumes under the influence of aerodynamic heating by the mainstream to which it is exposed in the absence of film cooling (Eckert, 1992).

Often the wall is cooled not only by the coolant injected into the boundary layer but also by convection on the other side. The heat flux q_w required to achieve a desired wall temperature, T_w, in the combined process is calculated with the equation;

$$q_w = h (T_w - T_{aw}) \quad (2)$$

In numerous experiments it was found that the heat transfer coefficient, h, on the solid wall downstream of the cooling holes can be approximated by the values occurring in normal convection without injection except in the immediate neighborhood downstream of the cooling holes. This does, however, not apply to the surface area with the cooling hole arrangement as it is studied in the present paper. Some information on those heat transfer coefficients, expressed in Stanton numbers, is found in Eckert (1984) based on measurements performed at Stanford University.

The focus of the present work is determination of the film cooling effectiveness of the endwall (or platform) to which the blades of a high-pressure turbine are attached. The end-wall cooling problem has attained greater importance in recent years since low aspect ratio and low solidity turbine designs have a higher ratio of end-wall to blade surface area. Mass (heat) transfer measurements have shown regions on the endwall with very high transfer coefficient that need protection (Goldstein and Spores, 1988). While considerable research has been done on three-dimensional flows in a turbine passage and their effects on the heat transfer coefficient at the end-wall, little published work is available concerning end-wall film cooling. Results of this investigation would also be complementary to the earlier film cooling, heat transfer, and flow visualization studies carried out in the same rig (Goldstein and Chen, 1985; Goldstein and Chen, 1987; Goldstein and Spores, 1988; Chen and Goldstein, 1992; Jabbari et al., 1992).

Blair (1974), in a pioneering work on turbine end-wall heat transfer, studied film cooling injection from a thin angled slot in the end-wall slightly upstream of the blade passage. Film effectiveness values were found to be quite high near the slot, but dropped off rapidly downstream. It was noted that, due to the secondary flows in the passage, the injected coolant is swept away from the pressure surface of one blade toward the suction surface of the other. Yamao et al. (1987) investigated the film cooling performance resulting from the leakage of sealing air through the flexible joints between adjacent blade platforms. Two slots were used to simulate these joints - one at the leading edge of the passage (similar to Blair) and one down the middle of the passage between the two blades. Sparse measurements of the adiabatic wall effectiveness showed agreement with Blair concerning injection through the leading edge slot. The intra-passage slot produced very little cooling effect on the end-wall except in the corner near the trailing edge of the blade suction surface. Granser and Schulenberg (1990) also measured the adiabatic wall effectiveness due to injection from a slot at the cascade leading edge and compared these results to a partially-parabolic numerical calculation.

Film cooling performance by discrete-hole coolant injection was investigated by Bourguignon (1985) and Sato et al. (1987). Bourguignon gives a general discussion on the effects of coolant injection on end-wall secondary flows and heat transfer coefficients. Sato et al. determined the adiabatic wall effectiveness distribution on the end-wall resulting from heated injection through an array of approximately 80 film cooling holes.

The present study is also concerned with end-wall film cooling by discrete hole injection. The adiabatic wall effectiveness distribution resulting from coolant injection through a small array of 14 film cooling holes is determined using mass transfer measurements and visualizations produced using ammonia gas and diazo paper. The use of only 14 injection holes leads to a vast reduction in the total mass flow of coolant when compared to the 80 holes used by Sato et al. Also, creative use of the ammonia-diazo visualizations in combination with the mass transfer measurements produces a reasonably detailed picture of the adiabatic wall effectiveness distribution on the end-wall.

EXPERIMENTAL APPARATUS AND MEASUREMENT TECHNIQUE

Experiments are conducted in a low-speed wind tunnel with a planar cascade of six scaled-up turbine blades. This is essentially the same apparatus described in Ito et al. (1978). The blades have a chord length of 169.1 mm, a span to chord ratio of 3.55, an inlet flow angle of 44.3°, and an outlet flow angle of 62.7°. Some details of the cascade and the film cooling hole arrangement are shown in Figure 1a. Fourteen 1.905 mm diameter film cooling holes are drilled through the end-wall between the middle blades at an angle of 25° with respect to the end-wall. The length to diameter ratio, L/D, for each holes is 15.77. Ten of the holes are intended for inline injection, and the other four for transverse injection. The coordinate location and angular orientation of each hole is also given. The smallest spacing between neighboring holes (holes 4 and 8) is 7.32 hole diameters. Sixty taps in the wall, 0.635 mm in diameter, are used to draw samples of the flow or measure wall pressures. The taps, designated by small solid circles in Fig. 1a, are aligned (within the design constraints) with the symmetry planes of the holes 1-10. An 8 mm clay fillet is formed at the junction of the blade and end-wall to eliminate the sharp corner and produce a more realistic end-wall geometry. Its extent on the end-wall is indicated by the dashed contour in Fig. 1a.

Film effectiveness values are obtained using a mass transfer technique described by Goldstein (1971). Air with a foreign gas tracer (a mixture of air with helium or sulfur hexafluoride) is injected into the mainstream and the resulting mass concentration of admixed gas on the impermeable wall (C_{iw}) is measured by analyzing gas samples obtained through the sampling taps in the end-wall. The corresponding impermeable wall effectiveness is defined as:

$$\eta_{iw} = (C_{iw} - C_i) / (C_j - C_i) \quad (3a)$$

In this experiment, $C_i = 0$, therefore:

$$\eta_{iw} = C_{iw} / C_j \quad (3b)$$

The temperature field in film cooling of an adiabatic surface and the concentration field in the mass transfer experiment on an impermeable surface are similar as long as the transport properties do not vary within the field (extension of Reynolds analogy between heat and momentum transfer). Subject to this restriction the two effectiveness parameters are then equal ($\eta=\eta_{iw}$). This condition is satisfied in the experiment with mixture of air and helium by the small amount of the tracer gas. Sulfur hexafluoride was mixed in

Injection Hole Coordinates			
hole #	X (mm)	Y (mm)	β (°)
1	64.4	186.9	70
2	81.0	172.4	70
3	99.2	157.1	70
4	117.1	139.9	70
5	72.6	149.3	70
6	85.3	142.6	70
7	100.4	135.3	70
8	116.1	126.0	70
9	129.0	119.5	70
10	145.0	109.1	70
11	100.0	117.3	20
12	115.5	109.4	20
13	129.5	102.0	20
14	144.3	93.8	20

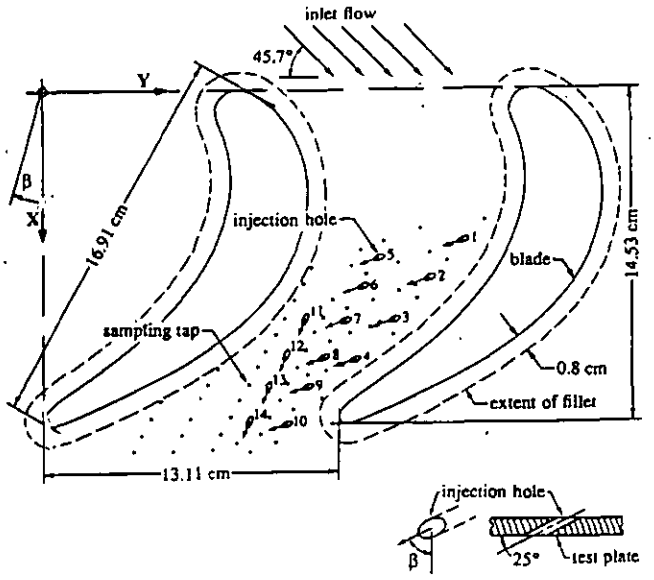

Figure 1a - Sketch of the test section

the secondary air stream to produce a density ratio, R, of the injected gas to the air in the mainstream near a value 2. This is characteristic of the density ratio of the cooling air to the hot mainstream gas in gas turbines. For this condition, the analogy between heat and mass transfer is only approximately fulfilled (Shadid, 1991).

The effect of the injected jets on the end-wall is visualized using ammonia gas and diazo paper in a manner similar to the tests of Dring et al. (1980). Commercial grade blue-line diazo paper is attached to the end-wall. Small amounts of ammonia and water vapor are added to the flow passing through the film cooling holes. Diazo paper contains an aromatic diazo compound and a coupler that, when allowed to react, will produce a colored dye. However, this reaction is suppressed by an acid embedded in the paper. In order to affect a color change, ammonia and water vapor are introduced to neutralize the acid and allow the coupling reaction to occur. The blue shadings left on the diazo paper, not only show the positions of the cooling jets and their interaction along the end-wall, they also relate to the amount of ammonium absorbed by the paper (mass transfer at the wall) which is due to the combined effect of the local ammonia concentration and the local mass transfer coefficient.

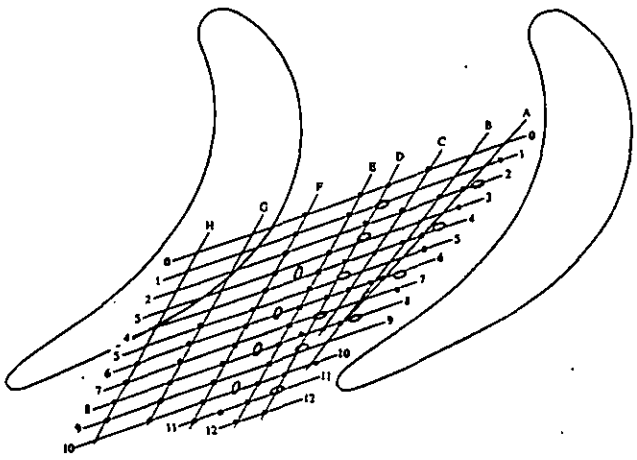

Figure 1b - Sampling tap and injection hole row designation

TEST CONDITIONS

Experiments are conducted for two approaching freestream velocities ($Re_c \approx 0.86 \times 10^5$ or 1.23×10^5), three nominal blowing rates ($\bar{M} \approx 1.0$, 1.5, or 2.0), and two density ratios ($R \approx 1.0$ or 2.0). The endwall boundary layer is tripped and for $Re_c = 1.23 \times 10^5$, a freestream velocity of 11.79 m/s, a boundary layer thickness of 28.51 mm, a displacement thickness of 3.10 mm, and a momentum thickness of 2.20 mm, are measured at a location 14.5 cm upstream of the blade's leading edge.

Over the endwall, the local freestream velocity varies due to the passage geometry. In Fig. 2, a contour plot of measured endwall pressure distribution is presented as :

$$(P_w - P_{i,s}) / (P_{i,t} - P_{i,s})$$

which is equivalent to :

$$[1 - (u_\infty / u_i)^2]$$

assuming potential flow through the passage. Contours shown in Fig.2 remain almost the same for both of the Reynolds number used in this experiment. Additional information regarding the flow field in the passage are available in Chung and Simon (1990), Chen and Goldstein (1992), and Jabbari et al. (1992).

Since the injection holes are fed from a single plenum chamber, it is clear that the flow rate through the film cooling holes is influenced by the endwall distribution. Therefore, to study the jets' performance collectively, rather than individually, a nominal blowing rate is defined as total coolant mass flow divided by total injection area and mass velocity of the approaching freestream :

$$\bar{M} = (\dot{m} / A) / (\rho_i u_i)$$

The nominal blowing rate, as indicated in Table 1, is, in fact, a weighted average of the injection hole blowing rates (M_j). The injection hole blowing rate is the mass flow rate of the coolant through each hole divided by the hole's flow area and the local freestream mass velocity :

$$M_j = (\dot{m}_j / A_j) / (\rho_\infty u_\infty).$$

The individual hole mass flow rate ($\dot{m}_j$) is evaluated from the pressure drop across the coolant passage and a discharge coefficient obtained by calibration. The local freestream velocity (u_∞) at each

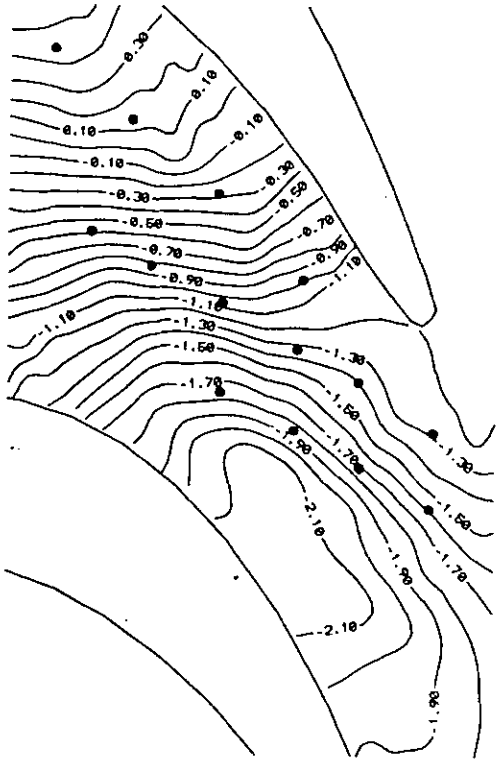

Figure 2 - Dimensionless pressure contours on the endwall $(P_w - P_{i,s}) / (P_{i,t} - P_{i,s})$ for Re_c=125000

injection hole is determined from the measured wall pressure distribution given in Fig. 2. In Table 1 values of M_j and u_∞/u_i are given for $Re_c = 1.23 \times 10^5$. It is important to note that the change in hole blowing rate (going from hole 1 to hole 14) at $\bar{M}$=1.07 is opposite that of $\bar{M}$=2.06 (as seen in Table 1). This is because of the diminishing difference between plenum chamber pressure and the endwall pressure at some hole locations, leading to a very small flow rate through those holes. In fact, reverse flow into the plenum chamber through holes 1 or 2 (see Fig. 1a) is a possibility at nominal blowing rates less than 1.0. For the values of Re_c examined, the dimensionless velocities (or the endwall pressure coefficient) show slight dependence on Re_c. This is also true for the hole blowing rates at a fixed nominal blowing rate.

DISCUSSION OF RESULTS

In Fig. 3 and Fig. 4 measurements of effectiveness for nominal blowing rates 1.0 and 2.0 are presented, respectively. The effectiveness (in percent) is written next to the sampling taps where it is measured. Plots of effectiveness variation along several rows (labeled in figure 1b) are shown in Figs. 5 and 6. Visualization of the trace of the film cooling jets on the endwall are obtained and presented in Figs. 7, 8, and 9. The uncertainties of the presented data, employing the method suggested by Moffat (1982), are; 5.7 % for film cooling effectiveness, 3.1 % for nominal blowing rate, and 2.9 % for density ratio. In the discussion that follows the injection holes and the sampling taps are referred to by the grid nearest to them (see Fig. 1b), for example, injection hole A2, D3, F6 (injection holes F4, F6, F8, F10 are actually between rows E and F) or sampling tap A2, C4, E6, F7, etc.

Table 1

Blowing Rates and Freestream Velocities at Injection Holes

$$\bar{M} = \frac{1}{14} \sum_{j=1}^{j=14} M_j (\rho_\infty u_\infty / \rho_i u_i)$$

$Re_c \approx 1.24 \times 10^5$				
	R=2.02		R=0.93	
Hole	$\bar{M}$=1.07	$\bar{M}$=2.06	$\bar{M}$=2.02	
j	M_j	M_j	M_j	u_∞/u_i
1 (A2)	0.35	2.30	2.53	0.73
2 (A4)	0.57	1.90	2.03	0.94
3 (A6)	0.69	1.67	1.71	1.14
4 (A8)	0.78	1.48	1.45	1.39
5 (D1)	0.75	1.55	1.55	1.28
6 (D3)	0.78	1.48	1.45	1.39
7 (D5)	0.80	1.43	1.39	1.47
8 (D7)	0.82	1.40	1.34	1.54
9 (D9)	0.82	1.40	1.34	1.54
10 (D11)	0.81	1.42	1.36	1.51
11 (F4)*	0.84	1.35	1.27	1.67
12 (F6)*	0.84	1.34	1.25	1.69
13 (F8)*	0.84	1.35	1.27	1.66
14 (F10)*	0.83	1.37	1.30	1.61

* Injection holes F4, F6, F8, F10 are actually located between rows E and F (see Fig. 1b)

Considering the large spacing between the injection holes A2, A4, and A6 (more than 7 hole diameters), one may expect that the effectiveness distribution downstream of these holes to resemble those previously reported for injection through a single or a row of holes (Goldstein, 1971). To verify this, comparison is made with the measurements reported by Pedersen et al. (1977) in Fig. 5. Pedersen's data are a centerline effectiveness for injection through a row of tubes (L/D=60) into a mainstream that has uniform velocity field outside its boundary layer. The tubes are spaced three diameters apart and are inclined at 35°. The present data are effectiveness along rows 2, 4, 6 (between rows A and D), for injection through holes A2, A4, and A6, into a mainstream with varying velocity field. The holes have L/D=15.77 and the injection angle is 25°. Although the mainstream flow fields and the injection geometries of the two sets of data are different, the comparison proves useful in interpreting some features of the present data.

For density ratio of about 2, and at low to moderate blowing rates, the difference between the present data and those of Pedersen et al. (1977) are not substantial. (Fig. 5a). Similar results are found along row 4 (M_j=0.57, I_j=0.16) though not shown in the figure. At higher blowing rates ($M_j \approx 2$), however, while the effectiveness values along row 4 (except close to the injection point) are close to those of Pedersen's, considerably lower values are measured along row 2 (Fig. 5b). This deviation seems rather peculiar and will be discussed later when the visualization results are examined.

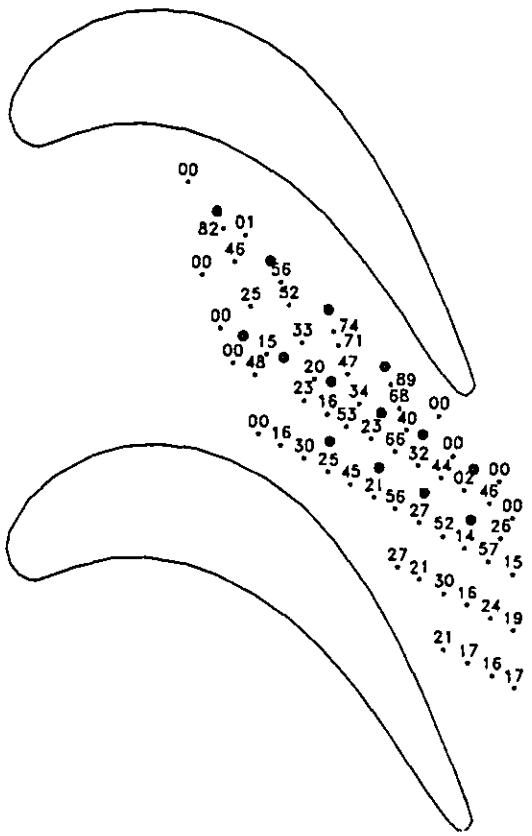

Figure 3 - Endwall effectiveness distribution
$\bar{M}$=1.07, R=2.01, Re_c=123600

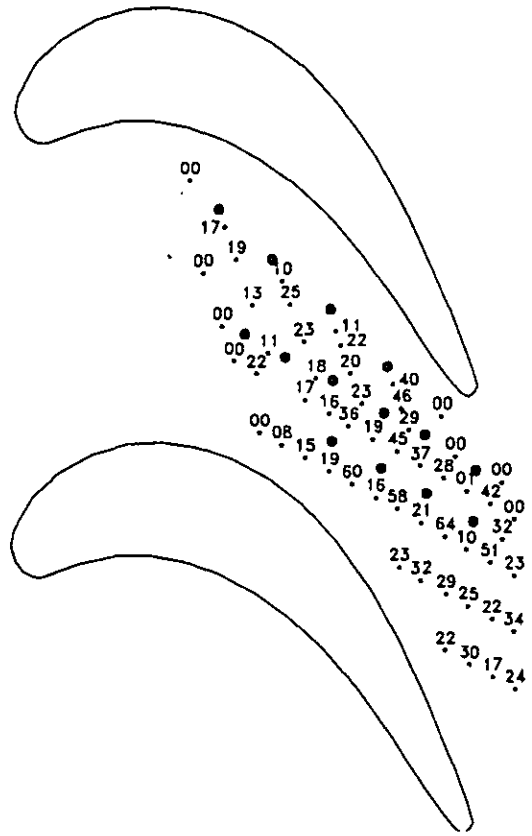

Figure 4 - Endwall effectiveness distribution
$\bar{M}$=2.06, R=2.02, Re_c=123100

Examination of the present effectiveness distribution along transverse rows (rows C, E, F, G shown in Fig. 6) reveals other peculiar features : For example, at the same distance downstream of injection holes D5, D7, D9, and for approximately the same blowing rates through them, the effectiveness downstream of injection hole D7 is much higher than those of holes D5 or D9 (compare readings of sampling taps E7, E5 and E9 along row E in Fig. 6). Along row F, a higher effectiveness is measured at sampling tap F2 -farther away from its aligned injection hole A2- than is measured at either of the taps F1 or F3 which are closer to their respective injection holes D1 and D3. While taps G6, G8, G10 (downstream of injection holes F6, F8, F10) indicate values of effectiveness that change with blowing rates ; the off-center taps G5, G7, and G9 (between the same injection holes) show approximately the same values of effectiveness independent of blowing rate.

It must be emphasized that the mainstream velocity field in this study is three dimensional and that the velocity varies, both in magnitude and direction, along and above the endwall. That is, each jet encounters a different velocity as it enters the mainstream and interacts with a varying flow field along its path. This could force changes on the jets and their trajectories, thus, altering the distribution of effectiveness. To provide information on the jet paths needed for the interpretation of the data, ammonium-diazo visualization of the jets' traces on the endwall is employed.

In Figs. 7 and 8 results of visualization for nominal blowing rates ($\bar{M}$) of 1.0 and 2.0 (density ratio ≈2) are presented. These figures correspond, respectively, to the data shown in Figs. 3 and 4.

In Fig. 9 visualization for $\bar{M}$=2 and R=0.93 is shown. In the visualization figures, traces of the film cooling jets on the endwall (blue colors) and their location relative to the sampling taps are visible. This shows which regions of the endwall are covered by the jets and how the boundaries of these regions have changed with a change in blowing rate and/or density ratio. Closer examination reveals details that help to explain the unusual features of the effectiveness data which were discussed earlier.

Focusing on the trace of the jet from hole A2 in Fig. 7, it is seen that the trace centerline is close to the first two sampling taps (A2 & B2) but farther downstream shifts away from the third (C2) and the fourth (D2) taps. This is what the data in Fig. 5a along row 2 (M_j=0.35) show ; the effectiveness at tap A2 (χ / D=1.7) and tap B2 (χ / D=7.1) are higher than those of Pedersen's but fall below them at taps C2 (χ / D=15.4) and D2 (χ / D=23.9). The near centerline effectiveness of the present study is higher than Pederson's possibly due its shallower injection angle (Goldstein and Stone, 1994) and its mainstream acceleration (Jabbari and Goldstein, 1978), and those at taps C2 and D2 are lower because they are off-centerline values. The displacement of the trace centerline from the sampling taps is more pronounced for row 2 in Fig. 8, revealing that the data for M_j=2.3 in Fig. 5b are also off-centerline effectivenesses, therefore, lower than the centerline values which may have been comparable to Pedersen's data (as are for row 4).

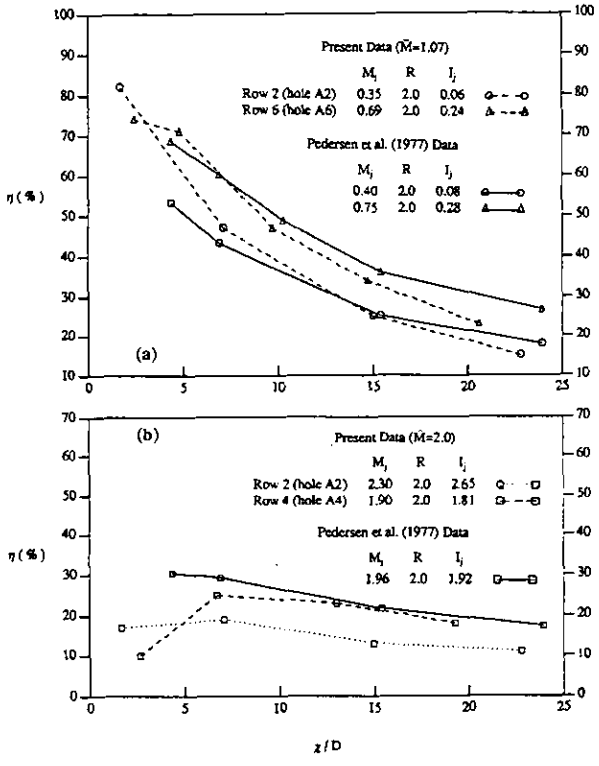

Figure 5 - Comparison of the present effectiveness data with those of Pedersen et al. (1977)

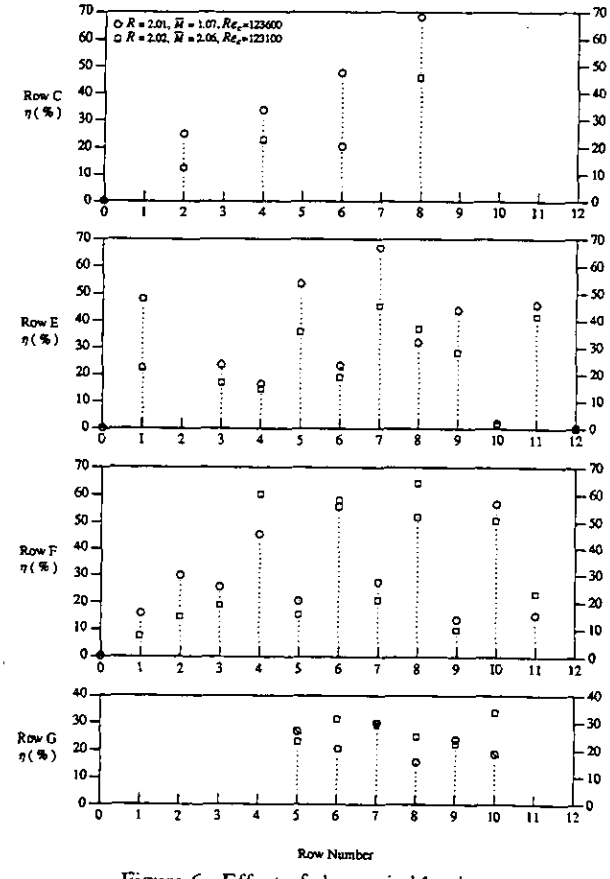

Figure 6 - Effect of change in blowing rate on effectiveness distribution

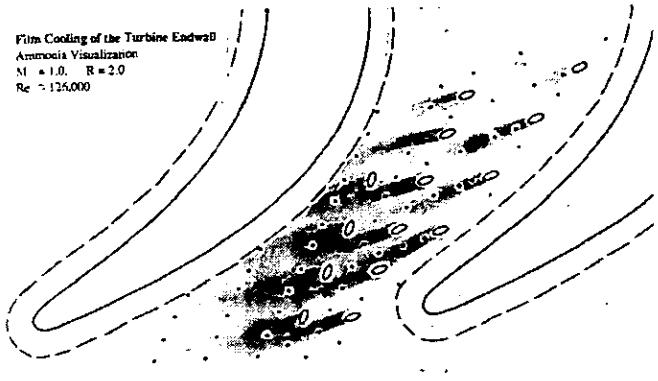

Figure 7 - Visualization of jet traces on the endwall
$\bar{M}$=1.0, R=2.0, Re_c=126000

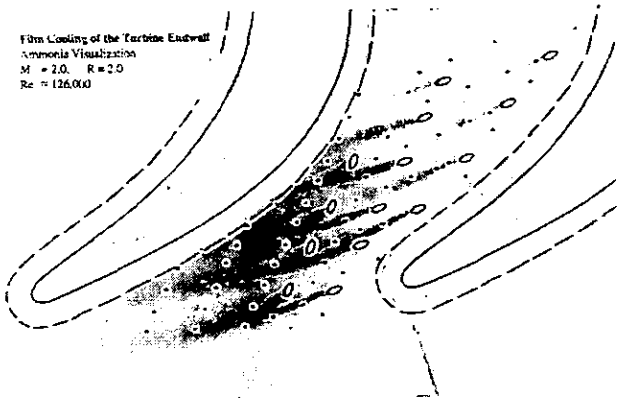

Figure 8 - Visualization of jet traces on the endwall
$\bar{M}$=2.0, R=2.0, Re_c=126000

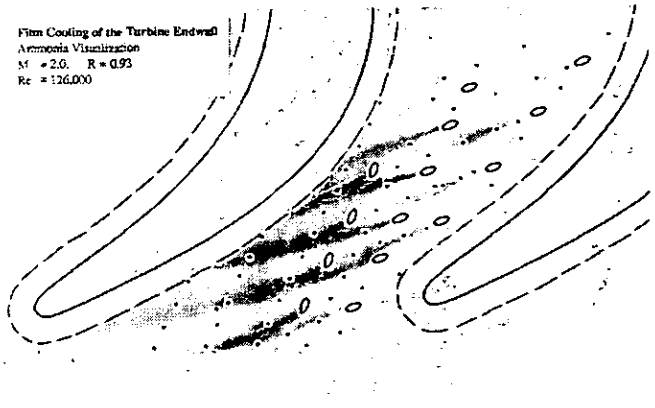

Figure 9 - Visualization of jet traces on the endwall
$\bar{M}$=2.0, R=0.93, Re_c=126000

Agreement / disagreement between effectiveness distribution along row 6 and data of Pedersen (see Fig. 5a) is explained in similar fashion. The lower effectiveness measured at tap A4 (χ / D=2.67) of row 4, the first data point of row 4 in Fig. 5b, appears to be a result of the jet not covering this tap because of its higher penetration and the tap's misalignment (see Fig. 8 and compare it with Fig. 7).

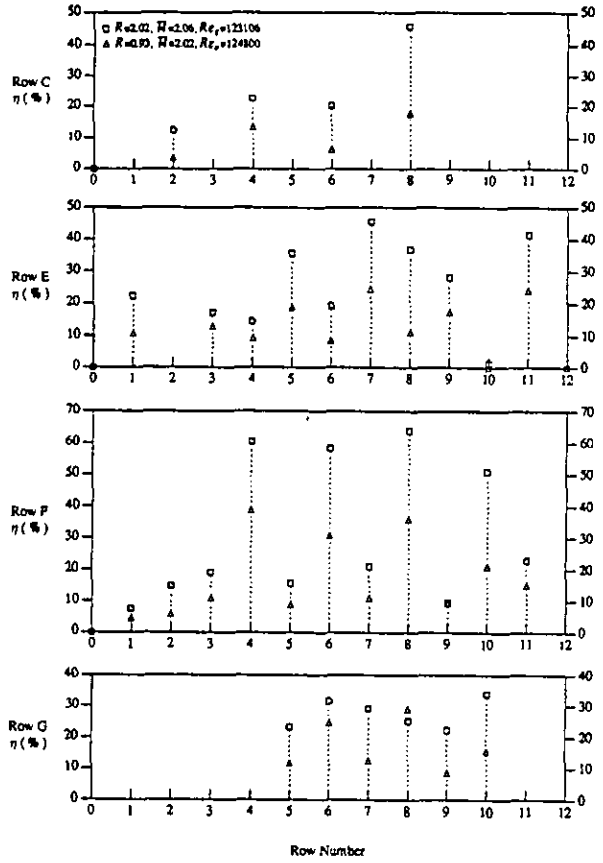

Figure 10 - Effect of change in density ratio on effectiveness distribution

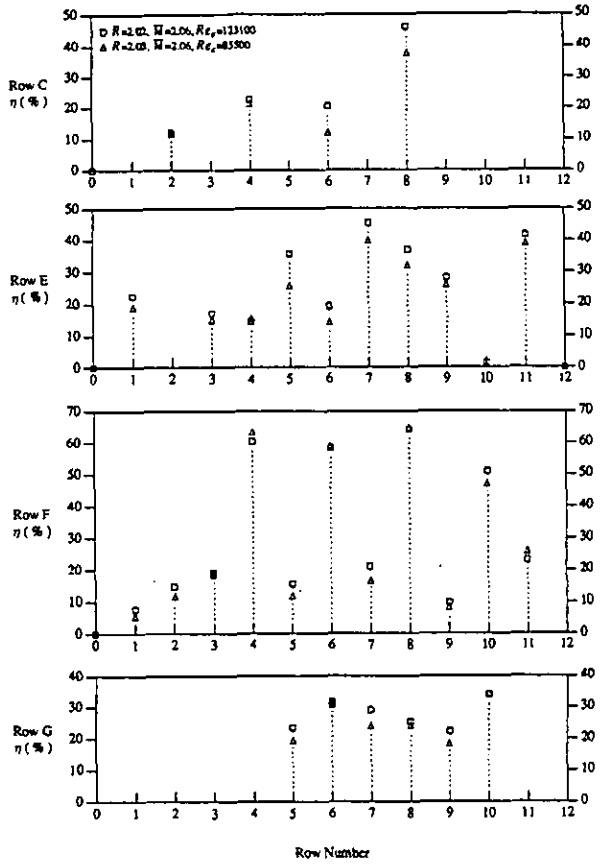

Figure 11 - Effect of change in Reynolds number on effectiveness distribution

Earlier, it was noted that effectiveness at tap E7 was higher than those at taps E5 and E9 (as seen in Fig. 6). Examination of the visualization results, particularly the one in Fig. 8, shows that the tap E7 is closer to the jet centerline than are taps E5 and E9. It is also interesting to note that some jets, for example D1 and D3 in Fig. 7, influenced by the local variation of the mainstream flow, follow a curved path and pass between the taps. In particular, the trace of jet D3 is not aligned with taps E3 and F3, instead, it is displaced upstream over tap F2 (Fig. 7). This explains the higher effectiveness that is measured at tap F2 relative to its neighbors F1 or F3. Noticeable in the visualization results are regions, without sampling taps in them, where two or more jets have merged. Judging from the strength of the intensity of color in these regions, and deducing from readings of taps F4, F6, and F8 in areas of comparable shade, very high levels of effectiveness prevail in these regions.

Comparison of traces in Figs. 8 and 9 show that jets of comparable blowing rates ($\bar{M} \approx 2$) but lower density ratio (higher momentum ratio) leave narrower traces on the endwall. This points to the higher penetration of the lower density jets into the mainstream, which leads to lower effectiveness at all of the measurement taps as are seen in Fig. 10. The reduction in effectiveness, however, is greater for taps closer to the jet centerline than those away from it (cf. readings of taps F4-F8 with the visualizations) which may indicate lateral as well as vertical change in the jet position. Moreover, the distribution of effectiveness along Row G has become more non-uniform at lower density ratio, indicating that the trajectories of the laterally injected jets (holes F4, F6, F8, F10) are slightly shifted by the change in the density ratio. When the jet traces (as seen in Figs. 8 and 9) and traces of the endwall flow obtained without injection (Jabbari et al., 1992) are compared, it is found that these jets do not follow the end wall flow direction; their paths lie closer to the potential flow direction in the passage. This, particularly, is more pronounced for the laterally injected jets (F4, F6, F8, F10).

The effect of the approaching flow Reynolds number on effectiveness, for the Reynolds numbers examined, are insignificant except close to the injection point downstream of jets A6, A8 and D5 (Fig. 11). Comparison of the corresponding visualization results indicates that only these jets are slightly displaced. This is in agreement with observation of Goldstein and Spores (1988) who found that a change in Reynolds number (of the same magnitude as in this study) had insignificant effect on the endwall mass transfer distribution. Also, as it was stated earlier, the endwall pressure distribution (Fig. 2) is not very sensitive to the change in Reynolds number. These indicate that the flow field near the endwall is not a strong function of Reynolds number in the range examined here.

All together, it is evident that the jet centerlines may depart from that of the injection hole depending on the jet's parameters and the mainstream velocity field and that the sampling taps (or thermocouples) aligned with the hole centerline may be indicating off-centerline values. Consequently, it becomes necessary to use other techniques, such as ammonium visualization or infra-red photography, to scan the entire endwall surface in order to obtain a true picture of the effectiveness distribution.

CONCLUSIONS

A wide variation in the level of film cooling effectiveness is observed on the endwall of a gas turbine blade. Several factors including large spacing between injection holes, variation in the mainstream velocity field, and displacement of the jet trajectories are responsible. Flow visualization results indicate that the jet centerline on the end wall, and thus the maximum effectiveness, are displaced with blowing rate and density ratio; suggesting that interpolation of the sparsely measured data should be done cautiously. The streamwise distribution of effectiveness, so far as the jets have not merged or changed lateral position, is predictable from the data available in literature. The color shade in the visualization results, particularly in regions where variation of the mass transfer coefficient is not appreciable, provides qualitative information on the effectiveness distribution.

ACKNOWLEDGEMENTS

The financial support of United Technologies (Pratt & Whitney) and contributions of Dr. T.J. Hajek and Dr. S. I. Tanrikut are gratefully acknowledged. This work was also partially paid for by the Air Force Office of Scientific Research.

REFERENCES

Blair, M., 1974, "An Experimental Study of Heat Transfer and Film Cooling on Large-Scale Turbine Endwalls," ASME 74-GT-33.

Bourguignon, A.E., 1985, "Etudes des Transfers Thermiques sur les Plates-Formes de Distributeur de Turbine avec et sans Film de Refroidissement," AGARD-CP-390.

Chen, P.H., Goldstein, R.J., 1992, "Convective Transport Phenomena on the Suction Surface of a Turbine Blade Including the Influence of Secondary Flows Near the Endwall," *Journal of Turbomachinery*, Vol. 114, PP. 776-787.

Chung, J.T. and Simon, T.W., 1990, "Three-Dimensional Flow Near the Blade/Endwall Junction of a Gas Turbine: Visualization in a Large-Scale Cascade Simulator," ASME 90-WA/HT-4

Dring, R.P., Blair, M.F., and Joslyn, H.D., 1980, "An Experimental Investigation of Film Cooling on a Turbine Rotor Blade," *Journal of Engineering for Power*, Vol. 102, PP. 81-87.

Eckert, E.R.G., 1992, "Similarity Analysis of Model Experiments for Film Cooling in Gas Turbines," *Warme- und Stoffubertragung*, Vol. 27, PP. 217-223.

Eckert, E.R.G., 1984, "Analysis of Film Cooling and Full-Coverage Film Cooling of Gas Turbine Blades," *Journal of Heat Transfer*, Vol. 106, PP.206-213.

Goldstein, R.J., 1971, "Film Cooling, " *Advances in Heat Transfer*, T.F. Irvine, Jr. and J.P. Hartnett, ed., Academic Press, Vol. 7, PP. 321-379.

Goldstein, R.J., and Chen, H.P., 1985, "Film Cooling on a Gas Turbine Blade Near the Endwall." *Journal of Engineering for Gas Turbines and Power*, Vol. 107, PP. 117-122.

Goldstein, R.J., and Chen, H.P., 1987, "Film Cooling of a Turbine Blade With Injection Through Two Rows of Holes in the Near-Endwall Region." *Journal of Turbomachinery*, Vol. 109, PP. 588-593.

Goldstein, R.J., and Spores, R.A., 1988, "Turbulent Transport on the Endwall in the Region Between Adjacent Turbine Blades," *Journal of Heat Transfer*, Vol. 110, PP. 862-869.

Goldstein, R.J. and Stone, L.D., 1994, "Row-of-Holes Film Cooling of a Convex and a Concave Wall at Low Injection Angles" manuscript

Granser, D., Schulenberg, T., 1990, "Prediction and Measurement of Film Cooling Effectiveness for a First-Stage Turbine Vane Shroud," ASME 90-GT-95.

Ito, S., Goldstein, R.J., Eckert, E.R.G. 1978, "Film Cooling of a Gas Turbine Blade," *Journal of Engineering for Power*, Vol. 100, PP. 476-481.

Jabbari, M.Y., Goldstein, R.J., 1978, "Effect of Mainstream Acceleration on Adiabatic Wall Temperature and Heat Transfer Downstream of Gas Injection," *Proceedings, 6th International Heat Transfer Conference*, (Toronto, Canada), Vol. 5, PP. 249-254.

Jabbari, M.Y., Goldstein, R.J., Martson, K.C., and Eckert, E.R.G., 1992, "Three dimensional flow at the junction between a turbine blade and the end-wall." *Warme- und Stoffubertragung*, Vol. 27, PP. 51-59.

Moffat, R.J., 1982, "Contribution to the Theory of Single-Sample Uncertainty Analysis," *Journal of Fluid Engineering*, Vol. 104, PP. 250-260.

Pedersen, D.R., Eckert, E.R.G., and Goldstein, R.J., 1977, "Film Cooling with Large Density Differences Between the Mainstream and the Secondary Fluid Measured by the Heat-Mass Transfer analogy," *Journal of Heat Transfer*, Vol. 99, PP 620-627. Also Pedersen's Ph.D. Thesis, Mech. Eng. University of Minnesota, 1972.

Sato, T., Aoki, S., Takeishi, K., Matsuura, M., 1987, "Effect of Three-Dimensional Flow Field on Heat Transfer Problems of a Low Aspect Ratio Turbine Nozzle," 87-TOKYO-IGTC-59.

Shadid, J.N., Eckert, E.R.G., 1991, "The Mass Transfer Analogy Tn Heat Transfer in Fluids with Temperature-Dependant Properties," *Journal of Turbomachinery*, Vol. 113, PP. 27-33.

Yamao, H., Aoki, S., Takeishi, K., Takeda, K., 1987, "An Experimental Study for Endwall Cooling Design of Turbine Vanes," 87-TOKYO-IGTC-67.